

The Northern High Time Resolution Universe Pulsar Survey I: Setup and initial discoveries

E. D. Barr,^{1,2,3*} D. J. Champion,¹ M. Kramer,^{4,1} R. P. Eatough,¹ P. C. C. Freire,¹ R. Karuppusamy,^{1,4} K. J. Lee,¹ J. P. W. Verbiest,¹ C. G. Bassa,⁴ A. G. Lyne,⁴ B. Stappers,⁴ D. R. Lorimer,⁵ B. Klein^{1,6}

¹ Max-Planck-Institut für Radioastronomie, Auf dem Hügel 69, 53121 Bonn, Germany

² Centre for Astrophysics and Supercomputing, Swinburne University of Technology, Mail H30, PO Box 218, Hawthorn, VIC 3122, Australia

³ Australian Research Council Centre of Excellence for All-Sky Astrophysics (CAASTRO), Mail H30, PO Box 218, Hawthorn, VIC 3122, Australia

⁴ Jodrell Bank Centre for Astrophysics, School of Physics and Astronomy, The University of Manchester, M13 9PL, UK

⁵ Department of Physics, West Virginia University, White Hall, Morgantown, WV 26506, USA

⁶ University of Applied Sciences Bonn-Rhein-Sieg, Grantham-Allee 20, 53757 Sankt Augustin, Germany

Received: –Accepted:

ABSTRACT

We report on the setup and initial discoveries of the Northern High Time Resolution Universe survey for pulsars and fast transients, the first major pulsar survey conducted with the 100-m Effelsberg radio telescope and the first in 20 years to observe the whole northern sky at high radio frequencies. Using a newly developed 7-beam receiver system combined with a state-of-the-art polyphase filterbank, we record an effective bandwidth of 240 MHz in 410 channels centred on 1.36 GHz with a time resolution of 54 μ s. Such fine time and frequency resolution increases our sensitivity to millisecond pulsars and fast transients, especially deep inside the Galaxy, where previous surveys have been limited due to intra-channel dispersive smearing. To optimise observing time, the survey is split into three integration regimes dependent on Galactic latitude, with 1500-s, 180-s and 90-s integrations for latitude ranges $|b| < 3.5^\circ$, $|b| < 15^\circ$ and $|b| > 15^\circ$, respectively. The survey has so far resulted in the discovery of 15 radio pulsars, including a pulsar with a characteristic age of ~ 18 kyr, PSR J2004+3429, and a highly eccentric, binary millisecond pulsar, PSR J1946+3417. All newly discovered pulsars are timed using the 76-m Lovell radio telescope at the Jodrell Bank Observatory and the Effelsberg radio telescope. We present timing solutions for all newly discovered pulsars and discuss potential supernova remnant associations for PSR J2004+3429.

Key words: (stars:) pulsars: general – (stars:) pulsars: individual: J1946+3417, J2004+3429

1 INTRODUCTION

It could be argued that no other astrophysical object has the ability to provide insight into as many fields of physics and astrophysics as the pulsar. The extreme conditions found in and around these objects make them unique natural laboratories for the study of subjects such as the equation of state of supra-nuclear matter (Demorest et al. 2010; Antoniadis et al. 2013), the behaviour of gravity in the strong-field regime (Kramer et al. 2006; Freire et al. 2012), the formation and evolution of binary

systems (Stairs 2004) and the existence and properties of gravitational waves (Hellings & Downs 1983). Therefore the discovery of new pulsar systems, through targeted or blind surveys, holds great scientific potential.

Pulsar surveys will in general always increase our understanding of the underlying source distribution and its properties, but it is the potential for the detection of rare and exciting systems, such as a hypothesised pulsar-black hole system (Narayan et al. 1991), that is the major driving force behind modern-day pulsar surveys. Several examples of such exciting discoveries can be found in surveys conducted within the last two decades. These include the discovery of the so-called ‘Dou-

* E-mail: ebarr@swin.edu.au

ble pulsar’, PSR J0737–3039A/B (Burgay et al. 2003; Lyne et al. 2004), which consists of two pulsars orbiting each other in a highly relativistic binary system; of PSR J1903+0327 (Champion et al. 2008), a rapidly rotating pulsar in a highly eccentric orbit, which has shed light on the evolution of hierarchical triple systems (Freire et al. 2011); of the ‘Diamond-planet pulsar’, PSR J1719–1438 (Bailes et al. 2011), with its Jupiter-mass CO white dwarf companion; and most recently of J2222–0137 (Boyles et al. 2013), a rapidly rotating pulsar with a massive companion, whose proximity to the Earth (~ 300 pc) makes it an exciting system, both for the measurement of post-Keplerian parameters and for the multiwavelength study of pulsar emission physics.

While targeted pulsar surveys, such as those that observe globular clusters (e.g. Ransom et al. 2005) or γ -ray point sources (e.g. Keith et al. 2011; Barr et al. 2012) tend to have a high discovery rate, they cannot produce an unbiased sample of the underlying population. To achieve a more complete picture of the true population distribution and the exotic systems it may contain, we must perform all-sky surveys.

In the past, blind surveys have been successful in detecting many new and exciting pulsar systems. Good examples can be found in the many surveys (e.g. Manchester et al. 2001; Burgay et al. 2006; Edwards et al. 2001) conducted using the 20-cm multi-beam receiver system of the Parkes Radio Telescope over the last 10 years. These surveys have been remarkably successful, not only discovering almost 60% of all known pulsars, but also some unique and fascinating objects. As well as the discovery of the aforementioned Double pulsar, these surveys have discovered six of the ten known double neutron star systems (DNS), pulsars with massive stellar companions (Johnston et al. 1992; Stairs et al. 2001) and the pulsar with the largest glitch (Manchester & Hobbs 2011). Furthermore, reprocessing of these data has led to the discovery of Rotating Radio Transients (RRATs; McLaughlin et al. 2006), a new class of pulsars that display bursty radio emission on varying timescales (see Keane et al. 2011, for a recent review).

The original Parkes multibeam surveys used a 96×3 -MHz channel analogue filterbank with a $250\text{-}\mu\text{s}$ sampling time. This relatively coarse frequency and time resolution resulted in a reduced searchable volume for narrow-pulse-width transients and millisecond pulsars (MSPs) due to dispersive smearing within individual channels (see Section 6.3.1). These limitations were compounded by a 1-bit digitisation scheme employed by the analogue filterbank. The limited dynamic range of 1-bit digitisation, although less sensitive to radio-frequency interference (RFI), acts to decrease the signal-to-noise (S/N) ratio of any pulsed or transient signal by $\sim 20\%$ (Kouwenhoven & Voûte 2001). While these surveys were state-of-the-art at their conception, affordable technology now exists to significantly improve on them. Recent advancements in field-programmable gate array technology and data transfer and storage techniques, have allowed for the use of tunable polyphase filterbanks capable of providing large numbers of high-resolution frequency channels and high sampling rates. These advances, combined with the development of a state-of-the-art 1.36-GHz multi-beam receiver for the 100-m Effelsberg telescope, have led to the commencement of the Northern High Time Resolution Universe (HTRU-North) survey, the motivation behind which is the discovery of

exotic and extreme pulsar systems, and the characterisation of the transient sky down to timescales of a few tens of microseconds.

The HTRU-North survey is half of a full-sky survey being undertaken using both the 100-m Effelsberg radio telescope in the northern hemisphere and the 64-m Parkes radio telescope in the southern hemisphere. Together, these surveys aim to achieve complete sky coverage at varying integration depths, with the deepest integrations along the Galactic plane (see Section 2).

The southern hemisphere half of the survey (High Time Resolution Universe; Keith et al. 2010) has been underway for several years, resulting in the discovery of more than 100 new pulsars, several of which are high-dispersion-measure MSPs (Bates et al. 2011; Keith et al. 2012) that were most likely undetected in previous surveys due to intra-channel dispersive smearing.

While Parkes has had a long, successful history with pulsar searches, the Effelsberg telescope has seen limited use as a pulsar survey instrument. This work marks the start of a new era of blind pulsar surveys with the Effelsberg telescope, building on the successes of Lorimer et al. (1999) and Barr et al. (2012) to clearly establish Effelsberg as a powerful instrument for pulsar searches.

In Section 2 we describe the observing strategy used in the HTRU-North survey. In Section 3 we describe the frontend and backend systems used at the Effelsberg radio telescope. In Section 4 we present analytical and empirical estimates of the survey sensitivity. In Section 5 we consider the expected pulsar yield as determined through Monte Carlo simulations of the Galactic pulsar population. In Section 6 we describe the data processing pipeline from acquisition to candidate selection. In Section 7 we present the timing solutions for all newly discovered pulsars and discuss potential supernova remnant associations for PSR J2004+3429. In Section 8 we present our conclusions.

2 SURVEY STRATEGY

The HTRU-North survey will be comprised of more than 1.5 million observed positions on the sky. To optimise the usage of our observing time, the HTRU-North survey is split into three complementary parts based on Galactic latitude.

The **high-latitude** section covers the sky at Galactic latitudes of $|b| > 15^\circ$ with short integrations of 90 s. The majority of sky covered by the high-latitude section has remained unsurveyed for more than 20 years, and so with the technical advances implemented in the HTRU-North survey we expect to discover many bright pulsars, which do not require long integration times to detect, and both Galactic and extragalactic transients (see Section 6). The near-isotropic distribution of MSPs expected to be discovered in this region will be of great use to current and future pulsar timing arrays for gravitational-wave detection (Foster & Backer 1990).

The **mid-latitude** section covers Galactic latitudes of $|b| < 15^\circ$ with 180-s integrations. This section of the survey probes the regions of the Galaxy most likely to contain undiscovered bright MSPs (again, vital for pulsar timing arrays). In the mid-latitude section, we also perform a shallow sweep of the Galactic plane. These observations are expected to discover any bright, longer-period pulsars.

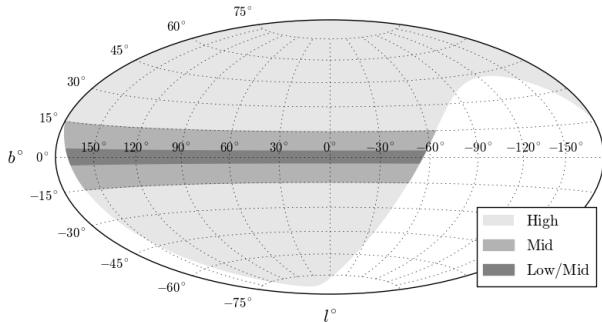


Figure 1. A Hammer projection of the Galaxy showing the survey area for all three regions of the HTRU-North survey. Note that the mid-latitude portion of the survey also incorporates the low-latitude survey region. For information on the parameters of each latitude region, please consult Table 1.

Finally, the **low-latitude** section covers Galactic latitudes of $|b| < 3.5^\circ$ with long integrations of 1500 s. These long integrations make this the deepest ever survey of the Galactic plane as seen from the northern hemisphere. Here we expect to discover many faint pulsars deep in the Galactic plane. This region is also where we have the greatest hope of discovering exotic systems such as double neutron stars and pulsars orbiting black holes, as these massive systems are expected to be close to their birth locations, given their relatively low ages (see e.g. Kramer et al. 2006).

For all latitude regimes, the integration times were chosen such that the limiting flux densities of the HTRU-North and HTRU surveys (Keith et al. 2010) were comparable. Table 1 shows integration times, data volumes and observational parameters for all parts of the HTRU-North survey.

It should be noted that portions of the survey area of the HTRU-North are currently being searched in the Green Bank Northern Celestial Cap survey (GBNCC) with the Robert C. Byrd Green Bank Telescope (Kaplan et al. 2012), the Arecibo L-band Feed Array survey for pulsars (P-ALFA) with the Arecibo Observatory’s William E. Gordon Radio Telescope (Cordes et al. 2006) and several up-and-coming pulsar surveys with the Low Frequency Array (LOFAR). Despite the GBNCC and HTRU-North covering essentially the same survey region, the lower observing frequency of the GBNCC, 350 MHz, results in the surveys probing different subsets of the pulsar population.

3 INSTRUMENTATION

All searching was performed using the 100-m Effelsberg radio telescope of the Max-Planck-Institut für Radioastronomie. Below, we describe the receiver and backend systems used to acquire observational data.

3.1 The 21-cm Effelsberg multi-beam receiver

The 21-cm Effelsberg multi-beam receiver consists of seven horns at the prime focus of the Effelsberg telescope. The horns

Table 1. Observational parameters for each latitude region of the HTRU-North survey. Both the bandwidth of the receiver ($\Delta\nu$) and the number of channels (N_{chans}) are given post RFI removal. For each region the minimum detectable flux density (S_{min}) for a pulsar with a 5% duty-cycle was calculated using the method outlined in Section 4. Here G_{central} and G_{outer} refer to the gains of the central in outer horns, respectively. Due to the physical location of the telescope, the survey has a minimum observable declination of -20° .

Survey	High	Mid	Low
Region	$ b > 15^\circ$	$ b < 15^\circ$	$ b < 3.5^\circ$
t_{obs} (s)	90	180	1500
N_{beams}	1,066,135	375,067	87,395
t_{samp} (μs)	54.61	54.61	54.61
$\Delta\nu$ (MHz)	240	240	240
$\Delta\nu_{\text{chan}}$ (kHz)	585.9	585.9	585.9
N_{chans}	410	410	410
G_{central} (K Jy^{-1})	1.5	1.5	1.5
G_{outer} (K Jy^{-1})	1.3	1.3	1.3
N_{samples} ($\times 10^6$)	1.6	3.3	27.4
S_{min} (mJy)	0.17	0.14	0.05
Data/beam (GB)	0.8	1.6	13.4
Data (total) (TB)	818.1	575.6	1117.8

are arranged in a hexagonal close-packed pattern around the central beam, with a beam separation of 0.25° . The central beam is circular with a beamwidth (full-width half-maximum) of 0.16° , while the outer beams have slight ellipticity with a corresponding circular beamwidth of 0.166° . Each of the seven horns has a bandwidth of 255 MHz centred on 1360 MHz and two polarisation channels, left- and right-hand circular for the central horn and orthogonal linear for the outer horns. Signals from the 14 channels are amplified in low-noise amplifiers, before undergoing down-conversion to an intermediate frequency of 150 MHz via heterodyning. After hardware RFI rejection we recover 250 MHz of useable band. This figure typically drops to ~ 240 MHz after software RFI rejection (see Section 6.2).

During the course of an observation the parallactic angle of the beam pattern on the sky changes with the telescope’s azimuth-elevation position. To keep the outer beams at constant Galactic latitude, the receiver box is rotated to maintain a constant parallactic angle.

The laboratory-measured receiver temperature of the central horn is 21 K, with the outer horns having temperatures of between 13 and 18 K.¹ The layout of the beam pattern on the sky and the tessellation unit for the survey can be seen in Figure 2.

3.2 The PFFTS backend

The Effelsberg Pulsar Fast-Fourier-Transform Spectrometer (PFFTS) backend was specially developed to meet the requirements of searching for pulsars with a wide-band, multi-beam receiver. The PFFTS is based on the AFFTS (Klein et al. 2012)

¹ The receiver temperatures for each horn, plus further information about the receiver system, can be found at <http://www.mpifr-bonn.mpg.de/effelsberg>.

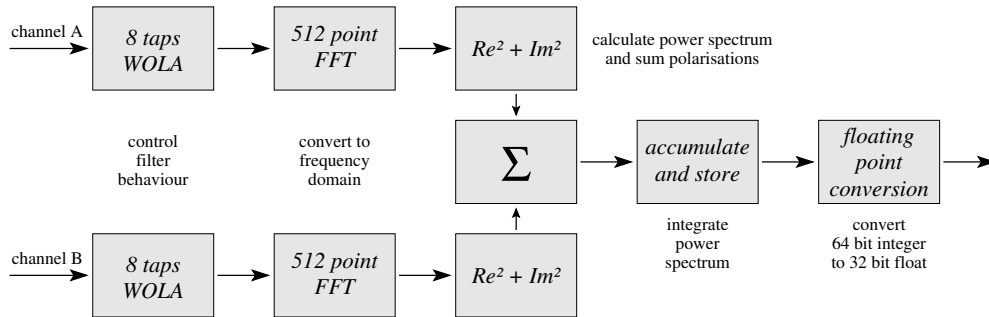


Figure 3. Block diagram of the FPGA signal processing pipeline. The digitised signals from both polarisation channels are individually transformed into the frequency domain by an 8-tap polyphase filter bank, implementing the weighted overlap-add (WOLA) method, before conversion to a power density spectrum representation. The polarisations are then summed, integrated over an adjustable time-period and converted from 64-bit integers to 32-bit floating point numbers.

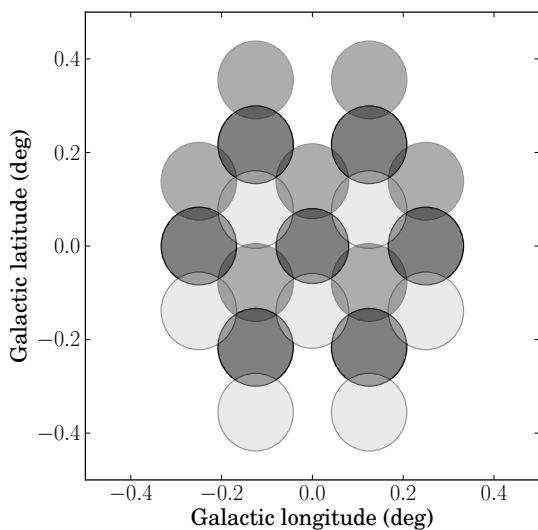


Figure 2. The beam pattern of the 21-cm Effelsberg multi-beam receiver on the sky. Shown are three pointings interleaved to make up a single tessellation unit for the survey. Circle diameters are given by the FWHM of each beam.

– an FFT spectrometer originally designed for spectral line observations. The backend combines seven identical electronic boards, each equipped with a high-speed analog-to-digital converter and a high-performance field-programmable gate array (FPGA). In “pulsar search” mode, the signal from each beam of the receiver is sampled by an analogue-to-digital converter (ADC) clocked at 600 MHz with 8-bit resolution. Following the ADC, the signal is processed by a 512-channel polyphase filter bank implemented on a Xilinx Virtex-4 FPGA. The output of the filter bank is further integrated by a factor of 32 and the two polarisations are quadrature summed. Processing in the FPGA is done at 32-bit resolution in order to avoid numerical overflow, resulting in an aggregate data rate of $\sim 38 \text{ MB s}^{-1}$ per beam. Finally, the data are transmitted through the on-board gigabit ethernet controller to seven sever-class computers attached to the FPGA boards.

4 SENSITIVITY

4.1 Analytic sensitivity

To estimate the minimum pulsed flux density, S_{\min} , observable by our survey, we use the modified radiometer equation (see e.g. Lorimer & Kramer 2005),

$$S_{\min} = \beta \frac{S/N_{\min} T_{\text{sys}}}{G \sqrt{n_p t_{\text{obs}} \Delta f}} \left(\frac{W_{\text{eff}}}{P - W_{\text{eff}}} \right)^{\frac{1}{2}}, \quad (1)$$

where the constant factor β denotes signal degradation caused by digitisation, which for 8-bit sampling is $\sim 0.01\%$, giving $\beta \approx 1$ (Kouwenhoven & Voûte 2001). The system temperature, T_{sys} , is the sum of the receiver temperature, T_{rec} , and the sky temperature T_{sky} . From flux density calibration measurements we find $T_{\text{rec}} = 21 \text{ K}$ for the central horn. The antenna gain, G , is 1.5 K Jy^{-1} at 1.36 GHz. Other parameters in this expression are the total integration time, t_{obs} ; the effective bandwidth of the receiver, Δf ; the number of polarisations summed, n_p , which for this survey is always two; the pulsar period, P ; the effective pulse width, W_{eff} ; and the minimum S/N ratio with which we can confidently make a detection, S/N_{\min} . Based on false alarm statistics (see e.g. Lorimer & Kramer 2005), $S/N_{\min} = 8$. Due to intra-channel dispersive smearing the effective pulse width increases with dispersion measure² (DM) as

$$W_{\text{eff}} = \sqrt{W_{\text{int}}^2 + \left(k_{\text{DM}} \frac{\Delta f_{\text{chan}}}{f^3} \text{DM} \right)^2} + t_{\text{samp}}^2, \quad (2)$$

where W_{int} is the intrinsic pulse width, t_{samp} is the sampling interval of the observation, f is the observing frequency, Δf_{chan} is the bandwidth of a single frequency channel and $k_{\text{DM}} = 8.3 \times 10^3 \text{ s}$. While scatter broadening will likely be the limiting factor on the DM depth to which we can detect short-period pulsars, the large uncertainty on its relationship with DM (Bhat et al. 2004) means that we disregard it when calculating expected sensitivities. For this reason, the sensitivity calculations here represent a best-case scenario. Figure 4 shows sensitivity curves for each region of the survey for a selection of DMs.

² Here, the dispersion measure is defined as the integrated column density of free electrons along the line of sight between observer and pulsar.

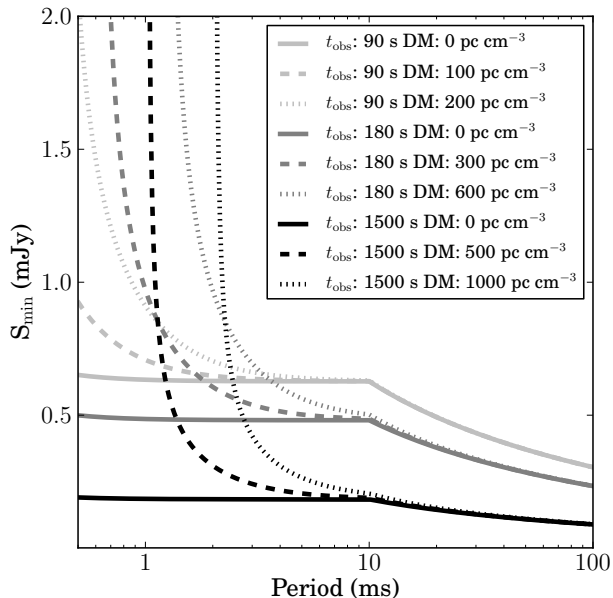


Figure 4. Theoretical minimum detectable flux densities (S_{\min}) vs. spin period for high-latitude, mid-latitude and low-latitude regions of the survey. For each region, the lines from left to right represent increasing dispersion measures. As the value of S_{\min} is dependent on the duty-cycle ($\delta = W_{\text{eff}}/P$) of the pulsar, we use the relation $\delta = P^{-1/2}$ (Kramer et al. 1998) to describe a more realistic duty-cycle distribution. As noted by Kramer et al. (1998), this relation does not hold for short-period pulsars. To account for this, a maximum duty-cycle of $1/3$ is imposed, resulting in the breakpoint seen at ~ 10 ms. For each integration length the sky temperature, T_{sky} , is given by the average sky temperature for the corresponding latitude range; 11 K for low latitudes, 8 K for mid latitudes and 5 K for high latitudes. A minimum detectable S/N ratio of 8 is imposed.

4.2 Pulsar redetections

Thus far, observations have been concentrated on the mid-latitude portion of the HTRU-North survey. Processing of the first 13% of these observations has led to the redetection of 93 known pulsars. To obtain an empirical confirmation of our survey sensitivity, observed S/N ratios were compared to S/N ratios predicted using published flux densities taken from the ATNF pulsar catalogue³.

Using the sky temperature model of Haslam et al. (1982), scaled with a spectral index of -2.6 (Lawson et al. 1987), and published pulsar positions taken from the ATNF pulsar catalogue, we calculated the expected S/N ratio for all redetections through rearranging equation 1. As the redetections did not lie in the centre of their discovery beam, S/N values were multiplied by a Gaussian offset factor, $q = e^{-(\theta/\phi)^2 \ln 0.5}$, to correct for off-axis gain decreases. Here θ is the pointing offset in degrees and ϕ is the beam half-width at half maximum.

To make the comparison more robust, only redetections that

³ <http://www.atnf.csiro.au/research/pulsar/psrcat/> (Manchester et al. 2005)

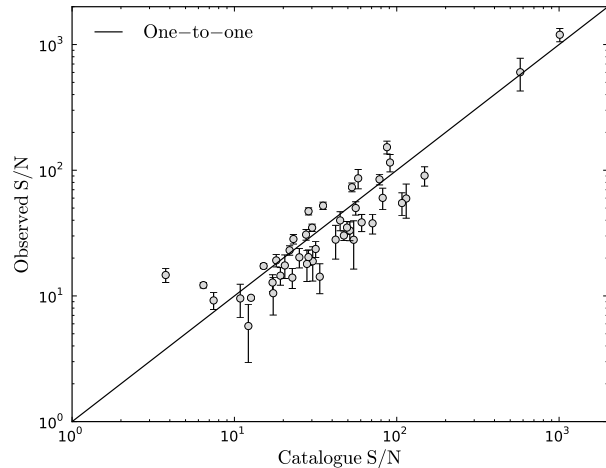


Figure 5. Observed S/N vs. expected S/N for redetected HTRU-North pulsars. Estimated S/N values are calculated using published flux densities taken from the ATNF pulsar catalogue, with a scaling factor for the offset of the pulsar from the bore-sight of the beam.

were within one beamwidth of the observed position were used. Redetection observations were also cleaned of RFI prior to S/N measurement (see Section 6.2). Figure 5 shows the observed S/N versus the expected S/N for the remaining sample of redetections.

As an independent test for sensitivity losses in the backend, timing observations from the Lovell telescope were also used to obtain S/N ratio measurements for the newly discovered pulsars from this survey. In all cases the S/N ratio measurement from the Effelsberg discovery observation agreed with the distribution of S/N ratio measurements obtained from the Lovell telescope timing data to within 1σ .

To verify that no pulsar had been missed by the survey, all pointings for which a known pulsar was within one beamwidth were examined. S/N ratios for these pulsars were estimated using the method outlined above. Of the pulsars with estimated S/N ratios above 8, five were undetected in the initial processing of the data. Folding the data for these pulsars with published ephemerides led to detections for two of the pulsars with S/N ratios below our detection limit. The three remaining undetected pulsars all have periods in excess of 2.5 s. Long period systems such as these, are often difficult to detect in short observations, as wider Fourier bins and large low-frequency components in the data act to suppress the pulsar signal. It should be noted that although these three pulsars were undetected in periodicity searches, one was detected through single-pulse analysis. These results confirm that the observing system is performing as expected, with no loss of sensitivity.

5 SIMULATIONS

To estimate the expected detection rate of the HTRU-North survey, Monte-Carlo simulations of the Galactic MSP and normal pulsar populations were performed using the model outlined in

Table 2. Simulated results for the total number of pulsars detected in each latitude region of the HTRU-North survey. To estimate the number of new discoveries from each region, the number of known pulsars expected to be detected in that region was subtracted from the simulated detection count.

Region	Detections		Discoveries	
	Non-MSPs	MSPs	Non-MSPs	MSPs
High-lat	145	28	29	7
Mid-lat	784	66	142	41
Low-lat	1123	81	642	64

Lorimer et al. (2006), with the PSRPOP⁴ software. To simulate the normal pulsar population, input model parameters were chosen as follows:

- Empirical period distribution taken from the probability density function of the known population.
- A log-normal pseudoluminosity distribution, defined at 1.4 GHz, with mean and standard deviation in log space of -1.1 and 0.9 , respectively (Faucher-Giguère & Kaspi 2006).
- An exponential distribution for the height above the Galactic plane, with a scale height of 330 pc (Lorimer et al. 2006).
- A radial distribution as described in Lorimer et al. (2006).
- A 6% duty cycle with dither given in Lorimer et al. (2006).
- The NE2001 Galactic free electron density model (Cordes & Lazio 2002).

The number of pulsars to be simulated was chosen such that the discovery rates of simulated versions of the Parkes Multi-beam Pulsar Survey (Manchester et al. 2001), the Swinburne Intermediate Latitude Pulsar Survey (Edwards et al. 2001) and its extension (Jacoby et al. 2009) and the Parkes High Latitude Survey (Burgay et al. 2006), matched those of their real counterparts.

To estimate the number of MSP detections expected from the survey, we used model ‘A’ of Lorimer (2012). This model updates the results of Lorimer et al. (2006) by taking into account Galactic MSPs found through recent high time- and frequency-resolution pulsar searches. Table 2 shows the results of the simulations and the expected discovery count for each region of the HTRU-North survey. The simulations suggest that the HTRU-North survey will detect ~ 1657 normal pulsars and ~ 153 MSPs, after taking into account pulsars co-detected in both the mid- and low-latitude portions of the survey. However, recent work on determination of the MSP luminosity distribution using pulsar detections from the HTRU survey (Levin et al. in prep.) has suggested that larger MSP yields may be expected.

6 DATA ANALYSIS

Processing of data collected for the HTRU-North survey is currently performed both on-site at the Effelsberg observatory and at the Max-Planck-Institut für Radioastronomie in Bonn. Data undergo pre-processing and RFI treatment before being processed twice, once in a ‘quick-look’ pipeline that operates on

reduced time- and frequency-resolution data and is sensitive to the majority of isolated pulsars in the data, and once in a full pipeline that incorporates searches for pulsars in compact binary systems. Below we describe all stages in the processing and archiving of data from the HTRU-North survey. It should be noted that the data analysis procedure reported here is only valid for mid- and high-latitude pointings from the survey. The analysis procedure for the low-latitude pointings will be presented elsewhere.

6.1 Pre-processing

Initially, data written in 32-bit format by the PFFTS backend are down-converted to 8-bit format for storage, transportation efficiency and software compatibility. During the conversion, the data in each frequency channel are clipped at the 3σ level⁵, allowing the data to be mapped to 8 bits with minimal loss in dynamic range. A by-product of this process is that the bandpass shape is removed from the data, as noisy channels are down-weighted and quiet channels are up-weighted with respect to one another. For purposes of RFI mitigation and completeness in the data archiving system, the original 32-bit data bandpass shape is stored.

6.2 RFI excision

Before the data are searched for pulsars, they are treated with several RFI excision methods to remove spurious signals of man-made origin. In the first stage of RFI removal, frequency channels with average power levels 3σ or more above the normalised mean across the original 32-bit bandpass are replaced with zeros. This reduces our sensitivity to weak, persistent, narrow-band RFI. The multibeam nature of the receiver allows for the application of a spatial filtering system to mitigate impulsive RFI in the data. Assuming all RFI that enters the multi-beam receiver is temporally coherent, we may apply a simple thresholding scheme to each data point to identify interference which appears in multiple beams.

The PFFTS is an adapted version of the AFFTS backend (Klein et al. 2012) used for HI observations at Effelsberg. As HI observations with the multibeam receiver do not require the high time resolution of pulsar observations, the AFFTS was not designed to have accurate synchronisation between individual beam servers. This can result in lags of up to a few milliseconds between the start of recording between different beams of the same pointing. Therefore, to perform multi-beam impulsive RFI excision, data must be cross-correlated to determine the absolute time offset. This process inherently relies on the presence of a multi-beam signal in the data which will produce a strong feature in the cross-correlation. In the cases where no such signal exists the impulsive masking section of the RFI excision is bypassed.

After an absolute reference has been determined for each pointing, each data point is compared across the seven beams. If the data point has a significance of 1.5σ in four or more beams,

⁴ <http://psrpop.phys.wvu.edu/>

⁵ i.e. all data points with values $> 3\sigma$ (three standard deviations above the channel mean) are reduced in power such that they have a value equal to the 3σ level of the original data.

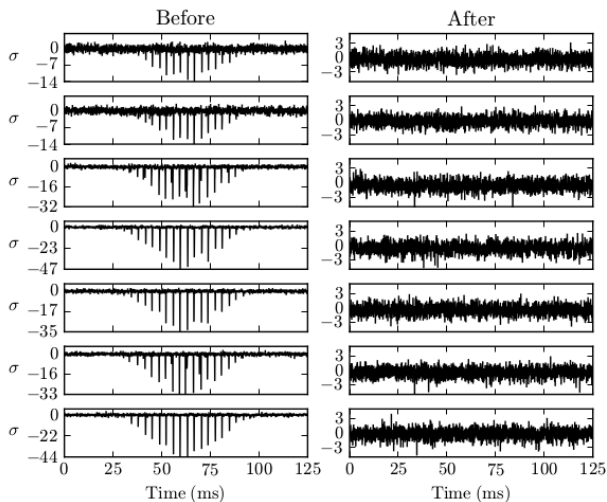


Figure 6. A the zero-DM time series for each beam of the multibeam receiver prior to (*left-hand column*) and post (*right-hand column*) RFI excision. The y-axis for each panel shows the number of standard deviation from the mean of the data. Here, the RFI appears as a decrease in power due to a combination of the low-noise amplifier response for very bright, narrowband signals and the clipping of each channel at the $3\text{-}\sigma$ level during conversion of the data from 32-bit floats to 8-bit integers.

it is replaced with Gaussian noise indistinguishable from the surrounding data and is logged for further analysis. Assuming that each channel is composed of Gaussian noise, the chance probability of removing a single ‘good’ data point is 0.00013%. The value of 1.5σ , as with all threshold values used in the RFI mitigation procedure, was chosen based on empirical tests of the mitigation procedure.

Once all beams have been compared, histograms of the RFI-flagged data points are created, both by time sample and frequency channel. By examining the number of RFI-affected data points in each frequency channel, we can isolate channels which have persistent impulsive noise. If the percentage of RFI-affected data points in a given channel is greater than 0.2%, the data in that channel are replaced by zeros. Similarly if more than 10% of the channels in a given time sample are RFI-affected, then all channels in the time sample are replaced by Gaussian noise, unless they have been previously replaced by zeros. An example of the zero-DM time series for each beam of the receiver before and after impulsive RFI excision can be seen in Figure 6.

To identify periodic signals in the pointing, the ‘clean’ data are collapsed along their frequency axis, with the resultant ‘zero-DM’ time series analysed in the Fourier domain (see Section 6.3.2). Fourier frequencies which appear in four or more beams with a $2\text{-}\sigma$ significance or greater are written to a ‘zaplist’ file that is used during periodicity searching and candidate sorting in the processing pipelines.

Typically the RFI excision process removes $\sim 4\%$ of the raw data. The majority of this is due to removal of the band edges and suppression of noisy frequency channels. After removal of these channels we recover an effective bandwidth of ~ 240 MHz.

6.3 Processing pipeline

Here we cover the main stages of the full processing pipeline used to analyse HTRU-North data. The pipeline is built around the PRESTO data analysis package (Ransom 2001). The quick-look pipeline is described in Section 6.4.

6.3.1 De-dispersion

Broadband electromagnetic signals propagating through the interstellar medium are subject to group-velocity dispersion. This results in a frequency-dependent time delay in the signal, with components at higher frequencies arriving at the observer before those at lower frequencies. As the degree to which the signal from an unknown pulsar is dispersed (its dispersion measure, DM), is not known *a priori*, we search 3240 trial DMs in the range $0\text{--}978\text{ pc cm}^{-3}$. Such a large number of trials allows for retention of the data’s highest possible time resolution at all DMs, as the minimum time delay between adjacent trials is limited only by the sampling rate and time delay between the top and bottom of a single frequency channel. It should be noted that to account for high-DM pulsars and transients the quick-look pipeline searches up to a maximum DM of 3000 pc cm^{-3} (see Section 6.4). At this stage in the analysis, the data are barycentred to remove the effects of the Earth’s rotation and motion in the Solar System.

6.3.2 Periodicity searching

Each of the 3240 time series created in the de-dispersion stage of the pipeline must be searched for periodic signals from isolated pulsars and pulsars in binary systems. To this end, the time series are discrete-Fourier-transformed to create a power spectrum for each DM trial. Often the power spectra contain strong low-frequency noise from long-period RFI or gain fluctuations in the receiver. To mitigate this, the power spectra are de-reddened through subtraction of an interpolated red-noise curve (Israel & Stella 1996). At this stage, Fourier frequencies which have been found to contain RFI through the excision process are suppressed in the spectra.

To reconcentrate power distributed through harmonics in the Fourier domain, the process of incoherent harmonic summing is used. Here, the spectrum is summed with a stretched copy of itself such that all second harmonics are added to their corresponding fundamentals. This process is repeated four times such that all power distributed in even harmonics up to the 16^{th} harmonic may be added to the fundamental (see e.g. Lorimer & Kramer 2005). To identify non-accelerated signals in the data, the spectra from each stage of the harmonic summing are searched for significant peaks.

In the case of pulsars in binary systems, the Doppler effect causes the apparent spin frequency of the pulsar to drift over the course of an observation, spreading the pulsar’s power in the Fourier domain. To reconstruct power smeared across multiple Fourier bins, we employ the ‘correlation technique’ of matched filtering as outlined in Ransom et al. (2002). The number of Fourier bins drifted by the signal, N_{drift} , and the binary acceleration of the pulsar, a_0 , are related by $a_0 = N_{\text{drift}} P c / t_{\text{obs}}^2$, where P is the spin-period of the pulsar, c is the speed of light

and t_{obs} is the observation length. To achieve sensitivity to accelerations of $|250| \text{ m s}^{-2}$ for a 1-ms pulsar, we search values of N_{drift} up to 27 for medium-latitude pointings and 7 for high-latitude pointings. Although the current value of $|250| \text{ m s}^{-2}$ is high enough to enable the survey to detect the most relativistic binary systems currently known, our assumption of a constant line-of-sight acceleration reduces our sensitivity to orbits that have $P_b \lesssim 10t_{\text{obs}}$ (Ransom et al. 2003).

6.3.3 Candidate sifting

To reduce the large quantity of candidates that periodicity searching produces, we apply a selection of thresholds and excision criteria. Initially, signals with the same period at different DMs are combined into a single candidate. At this stage any duplicate candidates are removed. As the relationship between S/N degradation and ΔDM (where ΔDM is the the offset from a pulsar intrinsic DM) for pulsars is well understood, we can excise candidates based on their DM characteristics. Candidates that are strongest at a DM lower than 2 pc cm^{-3} or do not show up at two or more consecutive DM trials are removed. Candidates that are lower significance harmonics of other candidates are also removed. Finally all candidates are sorted by significance to be passed to the folding algorithm.

It should be noted that all candidate sifting is done on a single-beam basis and no information from the other beams of the same pointing is used in determining the most pulsar-like candidates. Although it adds an extra layer of pipeline complexity, it is expected that future re-processings of the survey will benefit from implementing spatial filtering techniques to reduce the number of spurious candidates from each pointing.

6.3.4 Folding and optimisation

To determine if a candidate is truly a pulsar, the data are phase-folded and de-dispersed at the period and DM found through candidate sifting. After the data are folded, both the period and the DM of the candidate can be optimised through searching a small range of values around the discovery values. The optimisation is tailored such that for faster-period candidates, smaller ranges in DM and period are searched. To reduce sensitivity to RFI, long-period candidates do not undergo DM optimisation.

All candidates with greater than $8\text{-}\sigma$ significance are folded. In beams where there are less than 50 candidates above $8\text{-}\sigma$ significance, candidates with greater than $6\text{-}\sigma$ significance are also folded such that there is a minimum of 50 folds. Limiting the number of folds in this way reduces the probability of missing pulsars in observations strongly affected by RFI, as all candidates with a significance above our detection threshold are folded.

6.3.5 Candidate viewing and ranking

To deal with the >80 million candidates the survey will produce, a suite of interactive plotting software coupled with a MySQL⁶ database has been developed. For each folded can-

didate, the database stores all the relevant statistics of that candidate. Through use of the viewing software, users may query the database to select candidates which satisfy certain criteria, before viewing those candidates in the parameter space of their choice. User rankings of each candidate are stored in the database, with highly ranked candidates marked for re-observation.

For someone with experience in candidate selection, taking on average two seconds to view each candidate, it would take five years without pause to view all candidates produced by the survey. To reduce the volume of candidates that must be inspected, we implement both an artificial neural network (ANN) and an automatic ranking algorithm in post-processing.

The PEACE (Pulsar Evaluation Algorithm for Candidate Extraction) software package (Lee et al. 2013, submitted) is used to generate automatic rankings for each candidate. Here, the software weights and combines a selection of scores, determined through analysis of the folded data, to generate an overall ‘likeliness-of-pulsar’ measure for each candidate. As the PEACE software is designed to detect pulsars that display expected properties, it is subject to selection bias against atypical systems.

ANNs are a class of computational techniques which attempt to emulate the decision making behaviour of a human mind. ANN have been successfully applied to candidate selection (e.g. Eatough et al. 2010; Bates et al. 2012) and have been shown to reduce the number of candidates required to be looked at by several orders of magnitude. To train the ANN, it is provided with a vector of ‘scores’, in this case generated by the PEACE software, for each candidate from a selection of both real and simulated pulsar signals and RFI. The use of ANNs must also be treated with care, as their sensitivity to pulsars which do not exhibit typical behaviour (e.g. pulsars which are intermittent, in binary systems or highly scintillating) is dependent on the composition of the data set used in training. Although both ANNs and PEACE are effective in determining whether a candidate is a pulsar or not, direct visual inspection of the candidates is still the primary method of pulsar identification. The rankings generated through visual inspection act as an absolute reference for all automatic ranking systems.

6.4 Quick-look pipeline

The aim of the quick-look pipeline is to perform a reduced version of the full pipeline that is capable of processing all acquired data between observing sessions. By keeping up-to-date with the observed data, we are able to monitor the performance of the receiver and backend systems, as well as maintain up-to-date knowledge of the RFI environment at the Effelsberg telescope.

Data passed to the quick-look pipeline are initially down-sampled by factors of four and two in time and frequency, respectively. Although downsampling reduces our sensitivity to short-period/high-DM pulsars, it increases the throughput of the pipeline by a factor of eight, allowing processing to be performed with limited resources at $1.6\times$ real-time. The data are de-dispersed to 406 trial dispersion measures in the range $0\text{--}3000 \text{ pc cm}^{-3}$. To perform multiple de-dispersions efficiently, we employ the method outlined in Keith et al. (2010), with the caveat that we must first reduce the data to 7-bit resolution to avoid integer overflow in the output data.

⁶ www.mysql.com

For each trial DM, two searches are performed: a Fourier-domain search for periodic, unaccelerated signals and a time-domain search for isolated pulses. The Fourier-domain search closely follows the methodology outlined for the full pipeline with the exception that no acceleration searching is performed.

6.4.1 Transient searching

To search for isolated pulses in the time domain, we follow a similar methodology to that outlined in Burke-Spolaor & Bailes (2010). Here, we use matched filtering to identify significant impulsive signals of varying widths. Signals with significance greater than 4σ are collated and compared across all DMs to determine whether a candidate obeys the cold plasma dispersion relation and to determine that candidate's optimal dispersion measure. As the data have already undergone spatial coincidence filtering during pre-processing, no event matching is required across beams.

Candidate detections from the transient search are viewed on a pointing-by-pointing basis, with interesting signals being followed-up using software that provides tools for interactive manipulation and viewing of the filterbank data. Follow-up in this manner is vital in determining if a signal is of astrophysical origin or is simply RFI. Although the transient search has detected many known pulsars, no previously unknown transients have so far been discovered.

The remaining steps of the quick-look pipeline follow the same process as the full pipeline, with the exception that candidates are stored independently of the MySQL database.

7 NEW PULSAR DISCOVERIES

Here we present the initial pulsar discoveries of the HTRU-North survey. So far the survey has discovered 15 pulsars including one MSP. All discoveries originate from the processing of the first 13% of the mid-latitude region of the survey.

Upon discovery, each new pulsar is timed by the Lovell radio telescope at Jodrell Bank observatory and the Effelsberg radio telescope. Pulse times-of-arrival (TOAs) are analysed with the TEMPO2 software package (Hobbs et al. 2006) to create phase-connected timing solutions for each pulsar. Tables 3 and 4 show the new pulsar discoveries with current timing solutions and derived properties. In the case of PSR J0555+3948 the short timing baseline precludes the accurate determination of both position and flux density. In this case, the position error is assumed to be equal to the half-width half-maximum of a single beam and the flux density measurement assumes the discovery position to be the true position. As period derivative (\dot{P}) and position are covariant over short timing baselines, the \dot{P} measurement for all pulsars with data spans smaller than one year should be treated with caution. Figure 7 shows integrated pulse profiles from coherently dedispersed observations with the Lovell telescope. All timing observations are conducted in the 21-cm band with centre frequencies of 1.36 and 1.53 GHz, and bandwidths of 400 and 200 MHz for the Lovell and Effelsberg radio telescopes, respectively.

Observations with the Lovell are performed ~ 2 -3 times per week until a preliminary timing solution for the pulsar can be

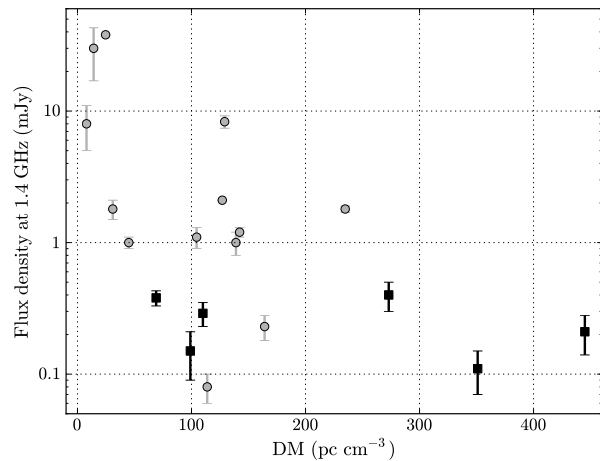


Figure 8. Comparison of the known pulsar population in the Orion-spur region, to pulsars discovered in this work. Grey circles show previously known pulsars with measured flux densities at 1.4 GHz. Black squares show pulsars discovered in this work.

determined. The cadence of observations is then reduced to ~ 1 observation every three weeks. After the pulsar's position has been improved through continued timing with the Lovell, higher precision timing observations with Effelsberg begin. Effelsberg observations for each pulsar occur on a monthly basis.

7.1 Orion-spur observations

To achieve complete coverage and statistics for a sample portion of the survey, mid-latitude pointings were targeted on the region $64.1^\circ < l < 71.9^\circ$, $|b| < 15^\circ$. In this direction the line-of-sight lies along the axis of the Orion spur up to a distance of ~ 3 kpc, and intersects with the Perseus arm and Outer arm at distances of ~ 6 kpc and ~ 10 kpc, respectively. These hydrogen-rich regions are known for star formation, and as such make excellent targets for pulsar searches.

The only survey of comparable sensitivity to have covered this area is the on-going P-ALFA survey (Cordes et al. 2006). Although the P-ALFA survey discovered five new pulsars in the region, the declination limit of $+38^\circ$ imposed by the Arecibo telescope limited its coverage. The Effelsberg telescope has no upper declination limit and so is capable of observing the entire Orion-spur region.

Data were processed in both quick-look and full pipelines and all candidates with folded profile significance greater than 6σ were viewed by eye. This has resulted in the discovery of six previously unknown radio pulsars including the eccentric binary MSP J1946+3417 and young pulsar J2004+3429, which are discussed in more detail in the subsequent sections.

Figure 8 shows the comparison between the newly discovered pulsars from this work and the known population in the region with measured flux densities at 1.4 GHz. It is clear that the pulsars discovered in this work have considerably lower flux densities at 1.4 GHz than their known counterparts. We also note that three of the newly discovered pulsars have DMs greater than

Table 3. Timing solutions for the first discoveries of the HTRU-North survey. Numbers in parentheses represent twice the formal 1- σ uncertainties in the trailing digit as determined by TEMPO2. Here, \dot{P} is the first derivative of the pulsar's spin-period. All parameters are measured w.r.t. reference epoch MJD 56100, unless otherwise stated. These parameters were determined with TEMPO2, which uses the International Celestial Reference System and Barycentric Coordinate Time. Refer to Hobbs et al. (2006) for information on modifying this timing model for observing systems that use TEMPO format parameters.

PSR	R.A. (h:m:s)	Decl. ($^{\circ}$:': $''$)	P (ms)	\dot{P} (10^{-15})	DM (pc cm $^{-3}$)	N_{TOA}	Data span (MJD)	Residual (μs)
J0212+5222 ^{†,‡}	02:12:52.2(6)	+52:22:45(13)	376.386292(1)	6.6(3)	38	17	56373 - 56477	73
J0324+5239	03:24:55.46(4)	+52:39:31.3(2)	336.620230291(3)	0.381(3)	119	64	55977 - 56478	309
J0426+4933	04:26:06.813(1)	+49:33:38.46(4)	922.474730055(2)	39.3444(2)	88	101	55844 - 56478	240
J0555+3948 [‡]	05:55(5)	+39:48(5)	1146.9058(2)		37	12	56373 - 56475	2904
J1905-0056 [‡]	19:05:27.9(1)	-00:56:37(5)	214.3943414(3)	1.07(7)	227	13	56356 - 56482	115
J1913+3732	19:13:27.887(3)	+37:32:12.30(7)	851.078948902(7)	1.3792(7)	69	77	55977 - 56479	321
J1946+3417	19:46:25.13182(6)	+34:17:14.677(1)	3.170139227806(2)	0.0000037(2)	110	156	56089 - 56477	5
J1959+3620	19:59:38.03(2)	+36:20:29.1(3)	406.08118100(1)	0.036(1)	273	116	55839 - 56481	3069
J2004+3429	20:04:46.97(3)	+34:29:17.7(5)	240.95264193(1)	206.825(4)	351	90	56069 - 56482	3476
J2005+3552	20:05:47.50(6)	+35:52:24.3(1)	307.94290464(2)	2.99(1)	445	55	56093 - 56480	512
J2036+2835	20:36:46.363(5)	+28:35:10.44(7)	1358.72676315(2)	2.090(2)	99	97	55873 - 56480	509
J2206+6151	22:06:18.119(6)	+61:51:58.10(3)	322.673549948(5)	0.397(4)	167	47	56028 - 56478	230
J2216+5759	22:16:05.22(3)	+57:59:53.7(3)	419.10226464(2)	69.048(2)	176	97	55838 - 56478	3710
J2319+6411	23:19:35.210(2)	+64:11:25.755(7)	216.01827884014(6)	0.1632(5)	246	56	56001 - 56475	75
J2333+6145	23:33:19.448(5)	+61:45:30.09(3)	756.899382059(7)	1.1761(6)	125	94	55838 - 56475	412

[†] co-discovered with the GBNCC survey (Lynch 2013).

[‡] parameters measured w.r.t. reference epoch MJD 56375.

Table 4. Further parameters for the first discoveries of the HTRU-North survey. Here, D_{DM} is the DM-derived distance, B_{surf} is the characteristic surface magnetic field strength, τ_c is the characteristic age, \dot{E} is the spin-down luminosity and l and b are the Galactic longitude and latitude, respectively. All DM-derived distances were calculated using the NE2001 Galactic free electron density model (Cordes & Lazio 2002), giving a likely uncertainty of $\gtrsim 20\%$ (Deller 2009).

PSR	l ($^{\circ}$)	b ($^{\circ}$)	D_{DM} (kpc)	Mean flux density at 1.5 GHz (mJy)	$\log_{10}(\tau_c)$ (years)	$\log_{10}(B_{\text{surf}})$ (Gauss)	$\log_{10}(\dot{E})$ (ergs s $^{-1}$)
J0212+5222	135.33	-8.52	1.5	0.9(4)	5.91	12.18	33.83
J0324+5239	145.09	-3.48	3.6	0.19(4)	7.15	11.56	32.60
J0426+4933	154.44	0.29	2.4	0.19(5)	5.56	12.79	33.30
J0555+3948	171.62	7.21	1.2	≥ 0.09			
J1905-0056	33.69	-3.55	5.9	0.11(1)	6.50	11.69	33.63
J1913+3732	69.10	12.13	4.0	0.38(5)	6.99	12.04	31.94
J1946+3417	69.29	4.71	5.1	0.29(6)	10.14	8.03	33.65
J1959+3620	72.44	3.44	11.5	0.4(1)	8.25	11.09	31.33
J2004+3429	71.42	1.57	12.5	0.11(4)	4.26	12.85	35.76
J2005+3552	72.71	2.14	> 18.0	0.21(7)	6.21	11.99	33.61
J2036+2835	70.41	-7.38	5.0	0.15(6)	7.02	12.22	31.51
J2206+6151	104.73	4.98	6.6	0.8(2)	7.16	11.53	32.62
J2216+5759	103.52	1.11	5.6	0.23(6)	4.98	12.73	34.57
J2319+6411	113.14	3.08	> 12.3	0.27(7)	7.35	11.26	32.77
J2333+6145	113.83	0.27	5.3	0.47(7)	7.00	11.98	32.03

250 pc cm $^{-3}$. The only other blind survey to have found pulsars in this region at such high DMs is the P-ALFA survey, which stresses the importance of using backends with high frequency resolution.

Of the high-DM pulsars discovered in the survey, PSRs J2005+3552 and J2319+6411 have DMs that are larger than the NE2001 Galactic free electron density model's (Cordes & Lazio 2002) expected maximum DM contribution along their respective lines of sight. This results in DM-derived distances that place the pulsars outside of the Galaxy. However, in both

cases the DM excess in the line of sight (75 and 13 pc cm $^{-3}$ for PSRs J2005+3552 and J2319+6411, respectively) falls within the expected uncertainties for the NE2001 model (Deller 2009).

7.2 PSR 1946+3417

Discovered as a 7- σ candidate in the full processing pipeline, PSR J1946+3417 has the honour of being the first millisecond pulsar discovered in the HTRU-North survey. With a spin period of 3.14 ms, binary period of 27 days and minimum com-

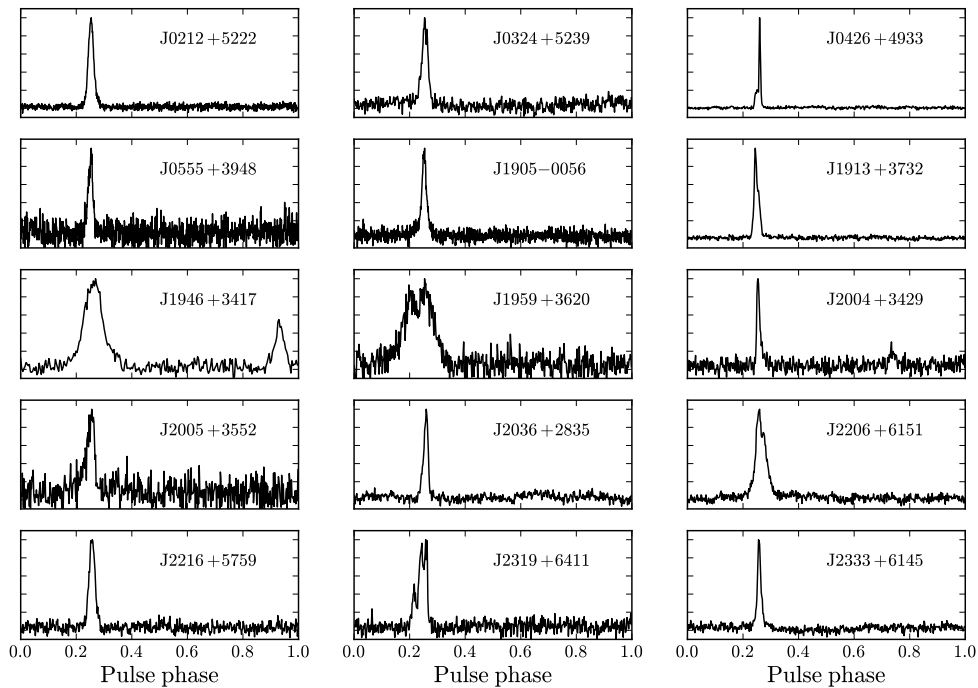


Figure 7. Integrated pulse profiles for the 15 newly discovered pulsars of the HTRU-North survey. The y-axes show the flux density of each pulsar on arbitrary scales. For the mean flux density of each pulsar, please refer to Table 4.

panion mass of $0.21 M_{\odot}$, the pulsar would at first glance appear to be normal MSP binary with a likely white dwarf companion. However, timing of the pulsar has shown the system to have a large eccentricity ($e \approx 0.14$). Assuming that the pulsar was spun-up through the accretion of mass from the current companion, one would expect the orbit to have been strongly circularised through tidal friction. Therefore, the high eccentricity of PSR J1946+3417 is somewhat anomalous. A possible explanation for the orbital configuration may be found in PSR J1903+0327 (Champion et al. 2008), a similar system which may have been formed in a hierarchical triple (Freire et al. 2011). An in-depth discussion of the possible origins of PSR J1946+3417 will be presented in Barr et al. (in prep.).

7.3 PSR J2004+3429

PSR J2004+3429 was initially discovered as an $11\text{-}\sigma$ candidate in a 3-minute pointing analysed with the quick-look pipeline. The pulsar has a spin period of 241 ms and a DM of 352 pc cm^{-3} . The radio profile of PSR J2004+3429 shows two components separated by 180° (see Figure 7), suggesting that the pulsar may be an orthogonal rotator. Using the NE2001 Galactic electron density model (Cordes & Lazio 2002) we estimate a distance to the pulsar of ~ 12.5 kpc. Analysis of pulsar distance measures by Verbiest et al. (2012) suggests that this distance is likely overestimated, with the real distance lying closer to 10 kpc. Timing with the Lovell radio telescope has led to a phase-coherent timing solution for PSR J2004+3429 that shows

it to have a large period derivative of 2×10^{-13} . For spin-down caused purely by the emission of magnetic dipole radiation, we find the pulsar to have a characteristic age of ~ 18 kyr.

7.3.1 SNR association

Considering the young age of PSR J2004+3429, it is highly likely that the pulsar is associated with a SNR. Using the SIMBAD astronomical data archive⁷, we find three published SNRs within a 2-degree radius of PSR J2004+3429: SNRs G069.7+01.0 (Kotthes et al. 2006), G070.7+01.2 (Kulkarni et al. 1992; Cameron & Kulkarni 2007) and G069.4+01.2 (Yoshita et al. 2000). The field also contains the candidate SNR G070.0+02.0 (Mavromatakis et al. 2009).

Small distance estimates to SNRs G070.0+02.0 (< 1 kpc, Mavromatakis et al. 2009), G069.4+01.2 (~ 2.5 kpc, Yoshita et al. 2000) and G070.7+01.2 (4.5 ± 1 kpc, Bally et al. 1989) appear to rule out any possible association with PSR J2004+3429. Using a revised Σ -D relation, which relates the surface brightness and diameter of SNRs to their distances, Case & Bhattacharya (1998) estimated a distance of ~ 14.4 kpc to SNR G069.7+01.0. This should be treated with care, as distance estimates via the Σ -D relation have an average uncertainty of $\sim 40\%$, and distance measurements to individual objects, especially those at large distances where popula-

⁷ <http://simbad.u-strasbg.fr/simbad/>

tion statistics are limited, may have much larger uncertainties (Case & Bhattacharya 1998). However, the large inferred distance is consistent with both the DM distance calculated for PSR J2004+3429 and the findings of Kothes et al. (2006), who note that SNR G069.7+01.0 is unpolarised at 1.42 GHz, possibly due to a large distance resulting in high beam depolarisation.

We calculate the separation of PSR J2004+3429 and SNR G069.7+01.0 to be $360 \pm_{82}^{131}$ pc, assuming that SNR G069.7+01.0 is located at the DM distance of PSR J2004+3429. For PSR J2004+3429 to have originated in SNR G069.7+01.0 would therefore require, assuming that the characteristic age is a close approximation of the true age, that the pulsar has a transverse velocity of the order 10^4 km s⁻¹. Using the model for the pulsar velocity distribution as found by Hobbs et al. (2005), we find the probability of PSR J2004+3429 having such a high transverse velocity to be consistent with zero. The large distance to PSR J2004+3429 makes any measurement of the pulsar’s proper motion highly unlikely. Unless PSR J2004+3429 is shown to have a large transverse velocity, we rule out any association with SNR G069.7+01.0.

7.3.2 *Gamma-ray observations*

PSR J2004+3429’s high spin-down luminosity ($\dot{E} = 5.7 \times 10^{35}$ ergs s⁻¹) marks the pulsar as a potential gamma-ray emitter (The Fermi-LAT collaboration 2013). To search for gamma-ray pulsations from PSR J2004+3429, *Fermi* LAT photons recorded between 2008 August 4 and 2013 May 10, with energies above 0.1 GeV, and from a 3° region of interest (ROI) around PSR J2004+3429 were phase-folded using the ephemeris shown in Table 3 and the *Fermi* plug-in distributed with the TEMPO2 package (Ray et al. 2011). To improve the chance of a detection, the phase-folded LAT data were restricted to ‘Source’ class events of the P7_V6 instrumental response functions. Furthermore, data taken during times when the rocking angle of the LAT exceed 52° or the Earth’s limb infringed on the ROI were rejected.

To determine if a statistically significant signal was present, a range of different angular and energy cuts was applied to the data in order to optimise the H-test parameter (de Jager & Büsching 2010). We tried maximum angular separation values between 0.1 and 3°, and minimum photon energies ranging from 0.1 to 1 GeV. None of the cuts applied resulted in a greater than 3σ significance. To remove any error introduced by uncertainties in our ephemeris, the same procedure was repeated using only data which was taken during the validity interval of our ephemeris. Again, no signal of greater than 3σ significance was found. Considering the large distance to the pulsar, it is feasible that the pulsar will become detectable when more LAT data are available.

8 CONCLUSION

We have described the instrumentation, observing strategy, sensitivity and expected results of the High Time-Resolution Universe North (HTRU-North) pulsar survey, the first major search for radio pulsars conducted with the 100-m Effelsberg radio telescope and the most sensitive survey ever to observe the entire re-

gion above +30° declination. The survey has thus far resulted in the discovery of 15 radio pulsars, of which 13 have been found above +30° declination.

Of the newly discovered pulsars, two are of particular note. PSR 1946+3417 is a highly eccentric MSP binary located in the Galactic field. This system will be presented in detail in a future paper. PSR J2004+3429 is a young pulsar with a characteristic age of ~18 kyr. We currently rule out that PSR J2004+3429 is associated with near-by SNR G069.7+01.0, due to the high transverse velocity required to place the pulsar at its current position with respect to the remnant in the time scale suggested by its characteristic age. Despite its high spin-down luminosity, we find no evidence of gamma-ray emission from PSR J2004+3429. This is most likely due to the large distance to the pulsar.

ACKNOWLEDGEMENTS

This work was carried out based on observations with the 100-m telescope of the MPIfR (Max-Planck-Institut für Radioastronomie) at Effelsberg.

Pulsar research and observations at Jodrell Bank Observatory have been supported through Rolling Grants from the UK Science and Technology Facilities Council (STFC).

JPWV acknowledges support by the European Union under Marie-Curie Intra-European Fellowship 236394.

PCCF and JPWV acknowledge support by the European Research Council under ERC Starting Grant Beacon (contract no. 279702).

DLR and MAM acknowledge support from WVEPSCoR and the Research Corporation for Scientific Advancement.

KJL acknowledges support from the ERC Advanced Grant “LEAP”, Grant Agreement Number 227947

REFERENCES

- Antoniadis J. et al., 2013, *Science*, 340, 448
- Bailes M. et al., 2011, *Science*, 333, 1717
- Bally J. et al., 1989, *The Astrophysical Journal*, 338, L65
- Barr E. D. et al., 2012, *Monthly Notices of the Royal Astronomical Society*, 429, 1633
- Bates S. D. et al., 2012, *Monthly Notices of the Royal Astronomical Society*, 427, 1052
- Bates S. D. et al., 2011, *Monthly Notices of the Royal Astronomical Society*, 416, 2455
- Bhat N. D. R., Cordes J. M., Camilo F., Nice D. J., Lorimer D. R., 2004, *The Astrophysical Journal*, 605, 759
- Boyles J. et al., 2013, *The Astrophysical Journal*, 763, 80
- Burgay M. et al., 2003, *Nature*, 426, 531
- Burgay M. et al., 2006, *Monthly Notices of the Royal Astronomical Society*, 368, 283
- Burke-Spolaor S., Bailes M., 2010, *Monthly Notices of the Royal Astronomical Society*, 402, 855
- Cameron P. B., Kulkarni S. R., 2007, *The Astrophysical Journal*, 665, L135
- Case G. L., Bhattacharya D., 1998, *The Astrophysical Journal*, 504, 761
- Champion D. J. et al., 2008, *Science*, 320, 1309

- Cordes J. M. et al., 2006, *The Astrophysical Journal*, 637, 446
- Cordes J. M., Lazio T. J. W., 2002, arXiv:astro-ph/0207156v3, 21
- de Jager O. C., Büsching I., 2010, *Astronomy and Astrophysics*, 517, L9
- Deller A. T., 2009, Ph.D. thesis, Swinburne University
- Demorest P. B., Pennucci T., Ransom S. M., Roberts M. S. E., Hessels J. W. T., 2010, *Nature*, 467, 1081
- Eatough R. P., Molkenthin N., Kramer M., Noutsos A., Keith M. J., Stappers B. W., Lyne A. G., 2010, *Monthly Notices of the Royal Astronomical Society*, 407, 2443
- Edwards R., Bailes M., van Straten W., Britton M., 2001, *Monthly Notices of the Royal Astronomical Society*, 326, 358
- Faucher-Giguère C., Kaspi V. M., 2006, *The Astrophysical Journal*, 643, 332
- Foster R. S., Backer D. C., 1990, *The Astrophysical Journal*, 361, 300
- Freire P. C. C. et al., 2011, *Monthly Notices of the Royal Astronomical Society*, 412, 2763
- Freire P. C. C. et al., 2012, *MNRAS*, 423, 3328
- Haslam C. G. T., Salter C. J., Stoffel H., Wilson W. E., 1982, *Astronomy and Astrophysics Supplement Series*, 47, 1
- Hellings R. W., Downs G. S., 1983, *The Astrophysical Journal*, 265, L39
- Hobbs G., Lorimer D. R., Lyne a. G., Kramer M., 2005, *Monthly Notices of the Royal Astronomical Society*, 360, 974
- Hobbs G. B., Edwards R. T., Manchester R. N., 2006, *Monthly Notices of the Royal Astronomical Society*, 369, 655
- Israel G. L., Stella L., 1996, *The Astrophysical Journal*, 468, 369
- Jacoby B. A., Bailes M., Ord S. M., Edwards R. T., Kulkarni S. R., 2009, *The Astrophysical Journal*, 699, 2009
- Johnston S., Lyne A. G., Manchester R. N., Kniffen D. A., D'Amico N., Lim J., Ashworth M., 1992, *Monthly Notices of the Royal Astronomical Society*, 255, 401
- Kaplan D. L. et al., 2012, *The Astrophysical Journal*, 753, 174
- Keane E. F., Kramer M., Lyne A. G., Stappers B. W., McLaughlin M. A., 2011, *Monthly Notices of the Royal Astronomical Society*, 415, 3065
- Keith M. J. et al., 2010, *Monthly Notices of the Royal Astronomical Society*, 409, 619
- Keith M. J. et al., 2012, *Monthly Notices of the Royal Astronomical Society*, 419, 1752
- Keith M. J. et al., 2011, *Monthly Notices of the Royal Astronomical Society*, 414, 1292
- Klein B., Hochgürtel S., Krämer I., Bell A., Meyer K., Güsten R., 2012, *Astronomy and Astrophysics*, 542, L3
- Kothes R., Fedotov K., Foster T. J., Uyaner B., 2006, *Astronomy and Astrophysics*, 457, 1081
- Kouwenhoven M. L. A., Voûte J. L. L., 2001, *Astronomy and Astrophysics*, 378, 700
- Kramer M. et al., 2006, *Science*, 314, 97
- Kramer M., Xilouris K. M., Lorimer D. R., Doroshenko O., Jessner A., Wielebinski R., Wolszczan A., Camilo F., 1998, *The Astrophysical Journal*, 501, 270
- Kulkarni S. R., Vogel S. N., Wang Z., Wood D. O. S., 1992, *Nature*, 360, 139
- Lawson K. D., Mayer C. J., Osborne J. L., Parkinson M. L., 1987, *Monthly Notices of the Royal Astronomical Society*, 225, 307
- Lorimer D., Kramer M., 2005. Cambridge University Press, Cambridge
- Lorimer D., Kramer M., Müller P., Wex N., Jessner A., Lange C., Wielebinski R., 1999, arXiv:astro-ph/9910569
- Lorimer D. R., 2012, arXiv:1210.2746
- Lorimer D. R. et al., 2006, *Monthly Notices of the Royal Astronomical Society*, 372, 777
- Lynch R. S., 2013, *Proceedings of the International Astronomical Union*, 8, 41
- Lyne A. G. et al., 2004, *Science*, 303, 1153
- Manchester R. et al., 2001, *Monthly Notices of the Royal Astronomical Society*, 328, 17
- Manchester R. N., Hobbs G., 2011, *The Astrophysical Journal*, 736, L31
- Manchester R. N., Hobbs G. B., Teoh A., Hobbs M., 2005, *Astron.J.*, 129, 1993
- Mavromatakis F., Boumis P., Meaburn J., Caulet A., 2009, *Astronomy and Astrophysics*, 503, 129
- McLaughlin M. a. et al., 2006, *Nature*, 439, 817
- Narayan R., Piran T., Shemi A., 1991, *The Astrophysical Journal*, 379, L17
- Ransom S. M., 2001, Ph.D. thesis, Harvard University
- Ransom S. M., Cordes J. M., Eikenberry S. S., 2003, *The Astrophysical Journal*, 589, 911
- Ransom S. M., Eikenberry S. S., Middleditch J., 2002, *The Astronomical Journal*, 124, 1788
- Ransom S. M., Hessels J. W. T., Stairs I. H., Freire P. C. C., Camilo F., Kaspi V. M., Kaplan D. L., 2005, *Science (New York, N.Y.)*, 307, 892
- Ray P. S. et al., 2011, *The Astrophysical Journal Supplement Series*, 194, 17
- Stairs I. et al., 2001, *Monthly Notices of the Royal Astronomical Society*, 325, 979
- Stairs I. H., 2004, *Science*, 304, 547
- The Fermi-LAT collaboration , 2013, ArXiv:1305.4385
- Verbiest J. P. W., Weisberg J. M., Chael a. a., Lee K. J., Lorimer D. R., 2012, *The Astrophysical Journal*, 755, 39
- Yoshita K., Miyata E., Tsunemi H., 2000, *Publications of the Astronomical Society of Japan*, 52, 867